Vortex Flow Driven Controls on Metastable Calcium Carbonate Formation via Integrated CO_2 Capture and Mineralization

Peilong Lu,[a] Prince Ochonma,[b] Rajashekhar Marthi,[a] Shardul Dinesh Prabhu,[a] Hassnain Asgar,[a] Yong Lak Joo[b] and Greeshma Gadikota [a,b*]

[a] School of Civil and Environmental Engineering, Cornell University, Ithaca, New York, 14853, USA

[b] Smith School of Chemical and Biomolecular Engineering, Cornell University, Ithaca, New York, 14853, USA

[*] Corresponding Author. Phone: +1 607-255-4796. E-mail: gg464@cornell.edu

Abstract

Precipitation is a critical step to produce inorganic powders with ultrafine size, and fine-tuned morphology. Precipitated calcium carbonate (PCC) is an important product of carbon dioxide mineralization due to its stable nature and wide application in industry. Particularly, a metastable form of calcium carbonate, vaterite, has been largely used in the fields of personal care and biomedical production due to its biocompatibility and tunable size and morphology. However, the inhomogeneity of conventional feed flow patterns heavily hinders the formation of PCC with desired properties. Herein, a Taylor-Couette Carbonate Conversion reactor (TC^3) is adapted to improve carbonate crystallization processes while producing carbonate particles with uniform particle size distribution and desired morphology. The formed vortex flows inside TC^3 can offer more significant mixing, higher surface-to-volume ratio, and increased mass transfer efficiency. In this study, many factors are investigated for the improvement of carbonate properties, such as reactant concentration, flow rate, agitation rate and reactor configuration. It is concluded that sphere-like vaterite particles with uniform size can be elaborately generated with vortex flows. Moreover, with high rotational strength and reasonable residence time, the obtained carbonate products tend to be more uniform size and higher in purity. More importantly, a couple of leachates which are prepared to serve as Ca sources from alkaline industrial residues and also examined in this study. The vortex-CO_2 technology addresses the societal need of utilizing multiple waste streams such as alkaline industrial residues and anthropogenic CO_2 to produce value-added products. This study sheds light on an efficient and commercially realizable process for producing value-added inorganic carbonates from captured CO_2.

Keyworks: Precipitated calcium carbonate; Taylor-Couette reactor; Taylor vortex; CO_2 mineralization, Metastable vaterite

1. Introduction

Carbon mineralization has been identified as a promising strategy for large scale carbon dioxide (CO_2) capture, utilization and storage (CCUS). This strategy is favored due to its potential to sequester CO_2. The strong CO_2 binding affinity of conventional sorbents, such as Ca- or Mg-based oxides, leads to the formation of value-added products.[1] In particular, calcium rich feedstocks are ideal for CO_2 mineralization due to the stable nature of the carbonate product ($CaCO_3$) and wide application in industry. $CaCO_3$ is an environmental-friendly material, and it is insoluble in water and undecomposable in natural environment.[2] More importantly, synthesized $CaCO_3$ products are widely used in a variety of fields such as cement, pigments, plastics and paints.[3] All these features and applications make the production of $CaCO_3$ by carbon mineralization technically feasible and economical viable.

In nature, $CaCO_3$ exists in three polymorphic forms, which are calcite, aragonite and vaterite in the order of stability.[4] These polymorphic forms usually exhibit distinct crystal structures and morphologies which are applicable in various fields.[3] Although vaterite is the least metastable product, there are several applications where it is preferred over the other crystalline structures due to its high porosity and higher solubility.[5, 6] On the basis of these properties, vaterite has been largely use in the fields of personal care and biomedical production. For instance, the demand for spherical vaterite particles is rising in the oral hygiene field because of their superior cleaning properties without being excessively abrasive;[6] nanoscale vaterite is widely utilized in dental care and regenerative medicine as bone cement, dental implants and scaffolds due to its superior mechanical strength compared to polymers.[7, 8] Moreover, vaterite nanoparticles exhibit a better performance as filler material in cement because they can accelerate the hydration of cement at the early stage.[9]

The precipitation to form the inorganic powders is a critical step in producing solids with ultrafine size and fine-tuned morphology. Traditionally, factors including reaction equilibria, solubility equilibria and ionic strength have been considered to mainly influence this precipitation.[10] However, controlling the flow dynamics of the feed mixing during crystallization can also significantly influence the particle properties of the precipitated product, including its particle size distribution, morphology and crystal structure.[11] These properties determine the final quality of the product. Particularly,

variations in mixing intensity, reactor configuration and geometry play a significant role in determining crystal size distribution.[12] For example, in a semi-batch configuration, it was observed that the mean particle size can be reduced when feed streams are closer to the impeller.[11] This is due to the different patterns of turbulence, created by the various distances between the impeller and the feed stream. Therefore, it is desired to develop a new reactor with a uniform flow pattern that can obviate the effect of inhomogeneity of mixing intensity.

Precipitated calcium carbonate (PCC) is a synthetic calcium carbonate product that has aroused great interest in both science and industry communities due to its biocompatibility, tunable size and morphology. The process of $CaCO_3$ precipitation occurs extremely fast, with time-scales ranging from less than milliseconds during intense mixing up to fractions of a second during low mixing.[13] This extremely fast precipitation rates hinder the use of regular reactors such as batch mode and T-mixer for morphological modulation due to their inherent feed flow design. One approach to obtain desired particles from precipitation is to reduce the mixing time scale with shortened contact. In addition, it is critical to develop reaction environments that can combine the advantages of different conventional reactors, including achieving lower volumes for similar space-time and conversion with plug-flow reactors (PFR) and more efficient reactant collision rates with continuous stirred tank reactors (CSTR). Achieving this integration will help overcome rate limiting steps associated with conventional reactor configurations.[13] In this context, the use of localized vortex flows in a Taylor-Couette (TC) reactor has been studied. The TC reactor design is expected to offer more significant mixing, higher surface-to-volume ratio, and increased mass transfer efficiency. As shown in Figure 1, the TC reactor typically consists of two coaxial cylinders, in which a rotating inner cylinder is inserted. Thus, an annular gap is formed, and various flow regimes can be created in this gap, which leads to unique flow conditions and shapes. The mixing conditions can be set by the axial flow and the rotational speed of the cylinders as well as geometry of the reactor itself.[14] It is important to note that in the TC reactor configuration, the feed-dependence can be weakened because the micro-mixing times are mainly influenced by inner cylinder rotations instead of feed stream flow. Also, the uniformity in the fluid dynamic conditions endows the TC reactor with the ability to modulate crystal size distribution.

It is promising to utilize Taylor vortices for the formation of uniform sized value-added inorganic carbonates. The special flow pattern favors products with desired properties via mixing of a CO_2-loaded amino acid solution and a Ca-bearing leachate solution. This vortex-CO_2 technology possesses the potential to address the societal need of utilizing multiple waste streams such as alkaline industrial residues (e.g., steel slag and coal fly ash) and sequester anthropogenic CO_2 to produce value-added products (Figure 1). The major motivation for this development of this technology are the costs associated with the treatment and landfilling of alkaline industrial residues (e.g., steel slag), and the opportunity cost of not using carbon tax credit ($35 per ton of anthropogenic CO_2).[15, 16]

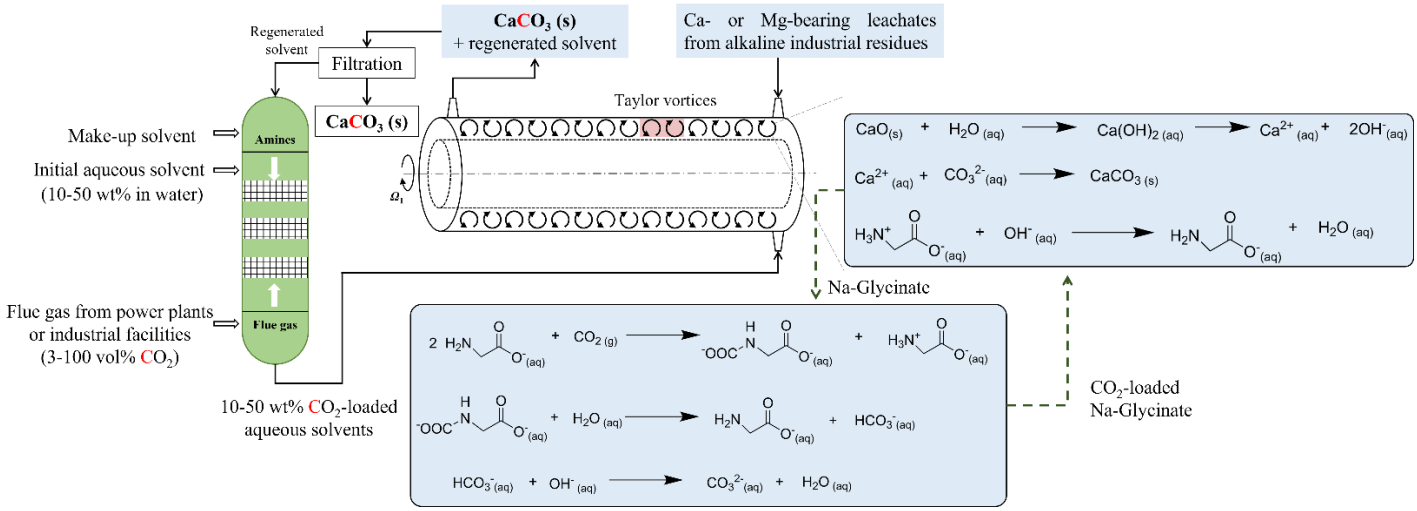

Figure 1. Integrated CO_2 capture and carbonate conversion approach with inherent solvent regeneration to produce metastable inorganic carbonates.

More specifically, we explore the role of vortex motion on calcium carbonate ($CaCO_3$) precipitation, using CO_2-loaded sodium glycinate as a precursor, and various Ca-containing solutions or leachates. Sodium glycinate (NaGly), has been extensively reported as an effective amino acid for CO_2 capture, and can be easily regenerated when brought in contact with a Ca-bearing solution leading to $CaCO_3$ precipitation.[17-21] Moreover, a Taylor-Couette Carbonate Conversion reactor (**TC^3,** see Materials and Methods for more details) is adapted to provide the unique opportunity to improve the carbonate crystallization processes towards producing carbonate particles with uniform particle size distribution and desired morphology. In the context of using a TC^3 reactor,

this study specifically investigates how flow dynamics influence the process of precipitation and properties of final $CaCO_3$ particles. The flow dynamics are impacted by parameters such as rotational speed, axial flow rate and residence time. Furthermore, multiple measurements are carried out using Ca solution and leachates obtained from real industrial wastes, i.e., blast furnace slag and construction demolition waste. We also discuss the effect of the presence of competing ions such as Mg in the leachate solutions on the formation of various calcium carbonate phases.

2. Materials and Methods

2.1 Chemicals: Sodium hydroxide (NaOH, Fisher Chemical), Glycine ($NH_2CH_2CO_2H$, 99%, Alfa Aesar) and Calcium chloride dihydrate ($CaCl_2 \cdot 2H_2O$, ~99%, MP) are used without further purification. Deionized water (18.2 MΩ·cm, Millipore) is used throughout the experiments.

2.2 Preparation of CO_2-loaded Sodium Glycinate (CO_2-NaGly) solution: 0.4 M sodium glycinate is prepared by dissolving equimolar compositions of NaOH (12.8 g) and glycine powders (24.0 g) in 800 mL deionized water. Subsequent, the prepared sodium glycinate solution is then bubbled with gaseous CO_2 (Bone Dry, Airgas) for 6 hours to obtain the CO_2-NaGly. In detail, NaGly reacts with CO_2 to produce CO_2-loaded NaGly (CO_2-NaGly), which supplies the carbonate ions (CO_3^{2-}) for precipitation (Eq. 1-4). Moreover, sodium glycinate is regenerated after solid carbonates precipitation and can be reused for subsequent CO_2 capture and mineralization.

$$CO_{2(aq)} + \mathbf{2NH_2CH_2COO^-_{(aq)}} = COO^-NHCOO^-_{(aq)} + NH_3^+CH_2COO^-_{(aq)} \quad (1)$$ [22]

$$COO^-NHCOO^-_{(aq)} + H_2O = \mathbf{NH_2CH_2COO^-_{(aq)}} + HCO^-_{3(aq)} \quad (2)$$

$$HCO^-_{3(aq)} = CO^{2-}_{3(aq)} + H^+_{(aq)} \quad (3)$$

$$CO^{2-}_{3(aq)} + Ca^{2+} = CaCO_{3(s)} \quad (4)$$

The kinematic viscosity of 0.4M CO_2-NaGly is 0.013 cm^2/s. Similarly, 1 M CO_2-NaGly is also prepared with the corresponding kinematic viscosity of 0.015 cm^2/s.

2.3 Preparation of $CaCl_2$ Solution: 0.2 M $CaCl_2$ is prepared by dissolving 23.5 g $CaCl_2 \cdot 2H_2O$ in 800 mL deionized water. The measured viscosity is 0.012 cm^2/s. 0.5 M $CaCl_2$ is also prepared with the measured viscosity of 0.013 cm^2/s.

2.4 Preparation of Waste *Concrete* leachate: Waste *concrete* is utilized to prepare this leachate. The calcium-rich leachate is prepared by mixing 50 g of waste concrete with 500 mL of acetic acid at room temperature for 3 h. The leachate is separated from the residue by vacuum filtration. The obtained leachate contains significant amount of Fe, Al and Si impurities which were removed by a pH swing process. Briefly, 1 M NaOH is added dropwise to the leachate until the pH reaches 9. Approximately 0.4 g of NaOH is consumed to perform the pH swing. In the end, the purified leachate contains 16000 mg/L of Ca^{2+}, as well as Mg (Fe: <20 mg/L, Mg: 660 mg/L, Al: <10 mg/L).

2.5 Preparation of *USFe* Leachate: USGS blast furnace slag (*USFe*) is used to prepare this Ca rich leachate used for this study. The major constituents present in *USFe* are determined using wavelength dispersion X-ray fluorescence (WD-XRF, Panalytical Axios) as shown in (Table S1). Detailed information on this approach can be found here.[23] Leaching is performed by dissolving 1 g of *USFe* slag in 50 mL of 1.5 M nitric acid at 40℃ with a 300 rpm stir. Under this acidic condition, Ca and Mg ions are extracted in large quantities, with Ca^{2+} and Mg^{2+} in solution reaching about 6254.50 mg/L and 1044.33 mg/L, respectively (determined by Inductively Coupled Plasma). The leaching of Ca and Mg is also accompanied by leaching of several other major elements including Si, Fe, Al, Cu and Mn whose presence has been reported to limit the kinetics and purity of $CaCO_3$ produced, hence a pH swing approach is utilized for selective precipitation of these elements, leaving behind a Ca & Mg rich solution at pH 9.

2.6 Preparation of Carbonate Products for Characterization: post-reaction, the final obtained suspensions are collected for further analysis. The suspensions are centrifuged at 4000 rpm for 10 minutes to separate solid carbonate products and regenerated solvent. Then, the solid products are washed with deionized water, and dried at 70 ºC overnight. The products are ground into powder for further analyses.

Finally, homogenous suspensions of carbonate particles in DI water are obtained via ultrasonication for 1 h before measuring the particle size of these products.

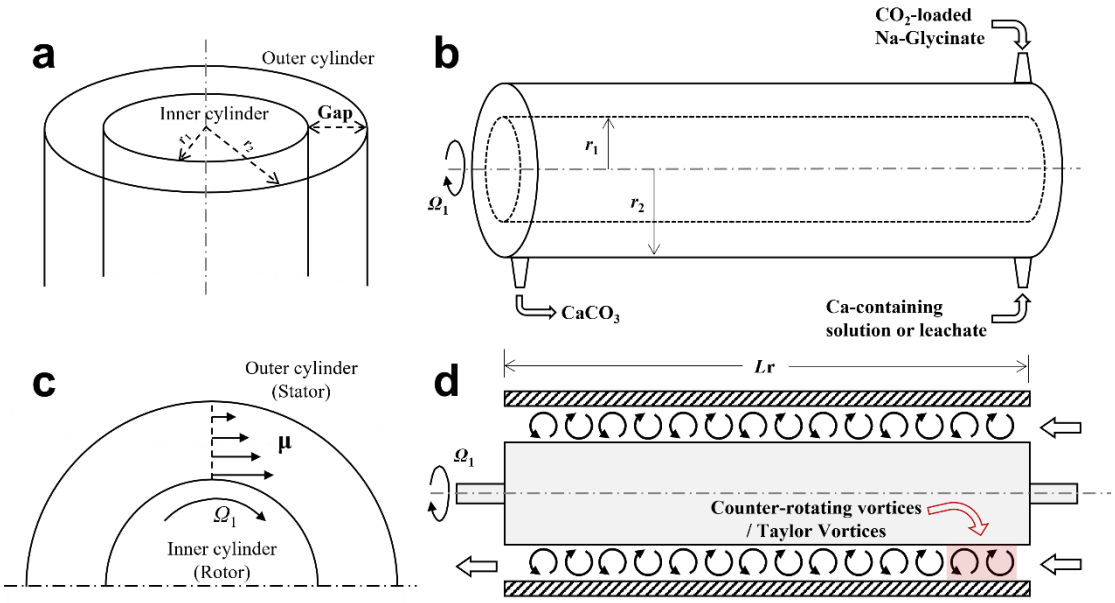

Figure 2. The schematic of the Taylor-Couette (TC) reactor configuration. (a) Two coaxial cylinders and the formed annular gap. (b) Schematic of calcium carbonate precipitation in the TC reactor. (c) Profile with the angular speed Ω_1 of the inner cylinder; μ refers to the resulting fluid velocity. (d) Cross-section drawn with the formation of Taylor vortices. [14, 24]

2.7 TC Reactor Setup: The Taylor-Couette Carbonate Conversion reactor (**TC^3**) setup is adapted in this study (Figure S1). It consists of two coaxial cylinders (Figure 2a & b), with a rotatable aluminum inner cylinder and a fixed Plexiglass outer cylinder. In detail, the rotatable inner cylinder is connected to a motor drive, which is controlled by a phase inverter that can provide rotational speeds in the range of 30 – 1500 rpm. In operation, it can generate Couette flow with a moving inner cylinder and a fixed shell (Figure 2d). Because of viscous forces, the fluid velocity profile consists of concentric layers whose velocity decreases away from the inner cylinder (Figure 2c). In addition, a peristaltic pump (Masterflex, 7523-30) with dual heads is used to supply the fluids to the reactor. The flow rate of the peristaltic pump is calibrated before use (Figure S2). A helical flow pattern can form with the addition of an axial flow. With rotational speed (Ω_1) increasing, it begins to form toroidal vortices in the TC^3 reactor. This gradually transforms into Taylor-vortex flow, which is the so-called Taylor-Couette flow (TCF).

Figure S1 displays a digital image of the developed TC^3 reactor in the lab. Physical specifications of the TC^3 reactor used in the current study are listed in Table 1**.** Besides, a tank reactor was also set up for comparison (Table 1).

Table 1. Dimensions of TC^3 reactor and tank reactor

TC^3 reactor (TC mode)		**Tank reactor (Batch mode)**	
Radius of inner cylinder, r_1 (cm)	2.29	Diameter of stirrer, cm	0.78
Radius of outer cylinder, r_2 (cm)	2.53	Length of stirrer, cm	2.18
Gap size, d (r_2-r_1) (cm)	0.26	Diameter of reactor, cm	4.65
Length of reactor, Lr (cm)	30.00	Height of reactor, cm	6.90
d/r_1	0.11	Volume of reactor, cm^3	117.24
r_1/r_2 (cm)	0.90		
Lr/d (cm)	116.28		

2.8 Details of TC^3 and Transition in Flow Pattern: Fluid dynamics play a crucial role in influencing the size, microstructure, crystallinity, and morphology of crystals during precipitation. These factors collectively determine the overall quality of the final product. Factors such as mixing intensity, reactor configuration, and geometry significantly impact the distribution of particle sizes. Therefore, by controlling the flow dynamics of the feed mixing both before and during the irreversible reaction, we are able to regulate particle properties.[12]

The primary hydrodynamic instability marks the Taylor-Couette flow (TCF) regime, as determined by the critical Taylor number (Ta_c). The Taylor number (T_a) is calculated by the following equation (Eq. 5).

$$T_a = \frac{2{r_1}^2 d^4}{{r_2}^2 - {r_1}^2}\left(\frac{\Omega_1}{v}\right)^2 \quad (5)$$

Where $\Omega_1$is the rotational speed of the inner cylinder, v is the kinematic viscosity of the solution, and $d = r_1 - r_2$ is the gap width. The superimposed axial flow is characterized by the axial Reynolds number (Re_z), as described by the following equation (Eq. 6).

$$Re_z = \frac{V_m d}{v} = \frac{Q(r_1 - r_2)}{Av} = \frac{Q}{\pi(r_2 - r_1)v} \quad (6)$$

Where V_m is the mean axial velocity, Q is the flow rate and A is the cross-sectional area of the channel.

The onset of instability, as specified by the T_a, relies on the geometry of the reactor and fluid properties. It includes the gap width ($d = r_2 - r_1$), the aspect ratio ($\Gamma = L/d$), and the ratio of the inner cylinder radius to the outer radius ($\eta = r_1/r_2$). A laminar azimuthal flow regime (known as Couette flow) occurs at low T_a, where the fluid is partially dragged along the walls of a cylinder (Figure 2c). Because of the viscous forces caused by inner friction, the velocity profile of fluid consists of concentric layers that progressively decrease in speed from the inner cylinder. When Ω_1 is increased beyond a critical rotational speed (denoted as Ta_c), a transition takes place from a laminar azimuthal flow to an axisymmetric cellular fluid motion. This occurs when the destabilizing centrifugal force surpasses the stabilizing viscous force.[25] Regardless of the presence of axial flow, a centrifugal instability begins, leading to the formation of toroidal vortices (counter-rotating vortices, Figure 2d) and the flow transforms into the Taylor-vortex flow (also refers to as Taylor-Couette flow). With an addition of axial flow, the resulting flow pattern over the cylinder transforms to a helical form, which varies depending on the Re_z.[14]

It is worth noting that the flow pattern in TC^3 is complicated since the axial flow significantly affects the critical Taylor number. It is pointed out that the increase in axial flow corresponds with an increase in the critical Taylor number. The presence of axial flow can diminish the dominance of centrifugal forces, leading to a significant delay in the onset of instability. Besides, the flow is complicated by turbulence due to entry and end effects. With increasing Re_z, the vortices can be distorted. In this study, the scope mainly focuses on vortex flow ($Ta > Ta_c$) with five various flow rates, Re_z = 10, 20, 30, 40, 50 (see Table 2 for more details). Moreover, under Taylor vortex flow, 4 different rotation rates are examined, 900, 1000, 1100, 1200 rpm at room temperature.

Table 2. Calculated *Rez* in this study.

No.	Pump-in flow rate (ml/s)	Residence time (s)	Re_z
20	1.88	59	10
40	3.76	30	20
60	5.64	20	30

80	7.52	15	40
100	9.40	12	50

2.9 Characterization of Products: All precipitates collected after reactions are centrifuged and washed with deionized water, followed by drying at 80˚C for 10 h. The particle size distribution is determined by Particle Size Analyzer (PSA 1190, Anton Paar) with the laser diffraction technology (Measurement range liquid: 0.04 µm to 2500 µm; Measurement range dry: 0.1 µm to 2500 µm). The structural features are examined using X-ray diffraction (XRD, Bruker D8 Advance ECO powder diffractometer) with a voltage of 40 V and a current of 25 A. XRD data is analyzed by Jade software, and crystalline species are identified via the International Centre for Diffraction (ICCD) database. The volatile components are determined using Thermogravimetric Analysis (TGA, TA Instruments, SDT 650). During TGA measurements, it is ramped from room temperature to 1000 ˚C with a rate of 10 ˚C/min under N_2 atmosphere (100 mL/min). The morphological features are imaged by Scanning Electron Microscope (SEM, Zeiss LEO 1550 FESEM). The concentration of metal cations in the liquid are measured by Inductively Coupled Plasma-Optical Emission spectrometry (ICP-OES, Spectro Analytical Instruments). The viscosity of solutions is determined by Viscometer (ViscoQC 300 Low range, Anton Paar). After measuring the viscosity, the kinematic viscosity is calculated by dividing the viscosity value by the density of the solution.

3. Results and Discussion

The properties of precipitation products highly depend on several factors such as reactant concentration, flow rate, agitation rate and reactor configuration.[12, 26] The nucleation and growth processes vary with the reactant concentration and flow pattern. Besides, the mixing of the solution significantly influences the reaction as well as the mass transfer processes. As a consequence, this study investigates the effects of varying reactants concentration, flow rate, and agitation (rotation and stir) on the morphology and size of the product particles. It is important to note that the pump-in flow rates of CO_2-loaded sodium glycinate (CO_2-NaGly) and $CaCl_2$ always remained the same during the precipitation, while different uniform rates are examined with various

rotational speeds in the TC mode (TC^3 reactor). For experiments carried out in the batch mode, the influence of stirring is also examined for comparison.

3.1 Effect of Ultrasonication for Agglomeration Mitigation

The overall precipitation process occurs through a combination of parallel and successive mechanisms that involve nucleation, growth, and secondary processes such as agglomeration, attrition, breakage and ripening.[3] Agglomeration, in particular, severely affects the resulting particle size distribution and morphology. Herein, ultrasonication was utilized to mitigate these effects. In this study, the mean size and size distribution are measured by light scattering instrument (PSA) with volume-based normalization.

The effect of ultrasonication on particle size distribution was investigated as shown in Figure 3. The peak of the particle size distributions slightly shifts towards the left, indicating smaller mean sizes (from mean size 5.70 to 3.40 μm) and become narrower after ultrasonication treatment. The broader size distributions, which can be reduced by ultrasonication treatment, could be affiliated to particle agglomeration over time during precipitation.[27, 28] As shown in Figure 3, the particle size distribution is found to be steady after 1 h of ultrasonication. It should be noted that the agglomeration is a common occurrence, and the effect plays a more significant role than crystal growth when determining the size distribution. Moreover, agglomerates flocked by chemical forces cannot be redispersed by ultrasonication, hence the size distributions after ultrasonication also showed a bimodality. From the bimodal distribution, it is also inferred that the first peak at 0.5 μm represents individual particles formed by nucleation and growth, as shown in the SEM images (as discussed later), whereas the second peak at around 4 μm represents agglomerates. It should be noted that in order to mitigate the effect of agglomeration, all particle size distributions and mean sizes in this study are measured after 1-hour ultrasonication treatment.

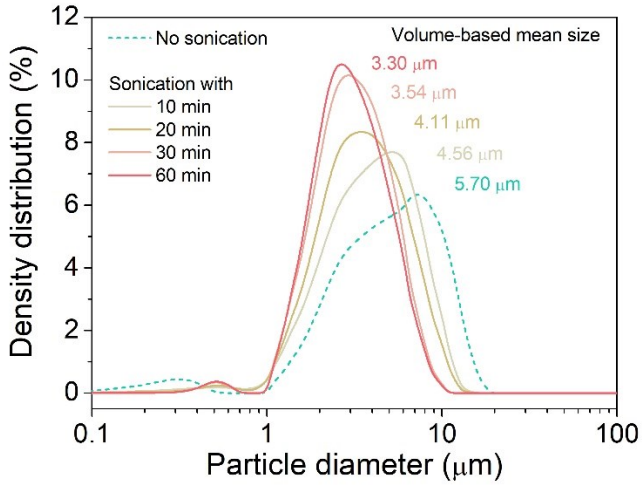

Figure 3. Effects of ultrasonication on particle size distribution of the calcium carbonate particle formed. The material is obtained after experiments are conducted in the TC mode under a rotational speed of 1100 rpm with a residence time of 30 seconds at a concentration of **1 M** CO_2-NaGly and **0.5 M** $CaCl_2$.

3.2 Effect of Mixing Mode and Initial Concentration

Supersaturation is the thermodynamic driving force of phase transition, and a prerequisite for the formation of particles. High levels of supersaturation are indispensable due to the highly nonlinear dependency of the nucleation rate on supersaturation.[3, 29] This is a measure of the system's thermodynamic offset from its equilibrium. For a binary salt such as calcium carbonate, supersaturation (S_c) can be calculated from the ion concentrations (Eq. 7) and the solubility product K_{sp} (Eq. 8).[29] For polymorphic materials, the most stable crystalline form has the lowest K_{sp}.[3] Moreover, supersaturation is one of the most significant factors determining the rates of nucleation and growth.[29] The precipitation process gets completed when primary particles are formed, and supersaturation is reduced to saturation. The next process, such as agglomeration, begins to change the particle size distribution within seconds.[29]

$$S_c = \sqrt{\frac{c_{Ca} c_{CO_3^{2-}}}{K_{sp}}} \tag{7}$$

$$K_{sp} = \left[Ca^{2+}{}_{(aq)}\right] \times \left[CO_3^{2-}{}_{(aq)}\right]; CaCO_{3(s)} \rightleftharpoons Ca^{2+}{}_{(aq)} + CO_3^{2-}{}_{(aq)} \tag{8}$$

The influences of mixing conditions on particle size distribution between TC mode and batch mode are observed to be even more significant at relatively higher supersaturation (concentrations of **1 M** CO_2-NaGly/**0.5 M** $CaCl_2$). As shown in Figure 4a, the particle sizes of products in the TC mode range between 0.2 – 10 µm with a rotational speed of 1000 rpm and 0.2 – 25 µm with 900 rpm. The corresponding volume-based mean sizes are 5.24 µm and 5.78 µm, respectively. In a sharper contrast, the particle sizes of the products produced by batch mode are in ranges of 0.1 – 35 µm (with stirring) and 0.1 – 64 µm (no stirring), respectively. Generally, the carbonate products generated under the TC mode exhibit a much narrower distribution and smaller mean size. The narrow distribution of particle size observed in TC mode indicates the ability to mitigate crystalline growth and agglomeration to some extent. However, the size modulation effect on various modes becomes less significant at lower concentrations (concentrations of **0.4 M** CO_2-NaGly/**0.2 M** $CaCl_2$). As shown in Figure 4b, the particle size of TC mode products was found to be in the range of 0.1 – 25 µm, which is much narrower than the sizes observed in of the batch mode under no stirring conditions (0.1 – 50 µm). Therefore, these results demonstrate that the special flow pattern obtained with the TC mode favors the formation of precipitated products with more uniform particle sizes, and the effect of mixing conditions on particle size distribution gets more significant with higher concentrations.

In addition, it is observed that an increase in reactant concentration tends to cause a shift towards the formation of larger particle sizes under conditions where there was no turbulence (12.47 to 20.22 µm in batch mode with no stir). However, in all cases with turbulence (TC mode and batch mode with stirring) and increase in reactant concentration caused a shift towards smaller particle sizes. A decrease from 7.72 to 5.24 µm, 8.84 to 5.78 µm, and 12.21 to 10.04 µm, was observed at TC mode 1000 rpm, TC mode 900 rpm, and batch mode 500 rpm respectively. These disparate behaviors may be explained by two different mechanisms. In general, higher supersaturation leads to more significant agglomeration because of the enhanced frequency of particle collisions.[30] Since supersaturation increases with concentration, higher concentration leads to larger particles size and distribution for batch mode without turbulence. However, nucleation plays a more important role in determining the particle size distribution when turbulence is introduced to the system because it can fairly improve mass transfer. Consequently, nucleation can be favored over the growth and

agglomeration. In the TC mode, the nucleation is more favorable than the particle growth.[3] As a result, higher level of supersaturation in this study tends to produce smaller particles. This explains the different behaviors for TC mode and batch mode with increasing supersaturation.

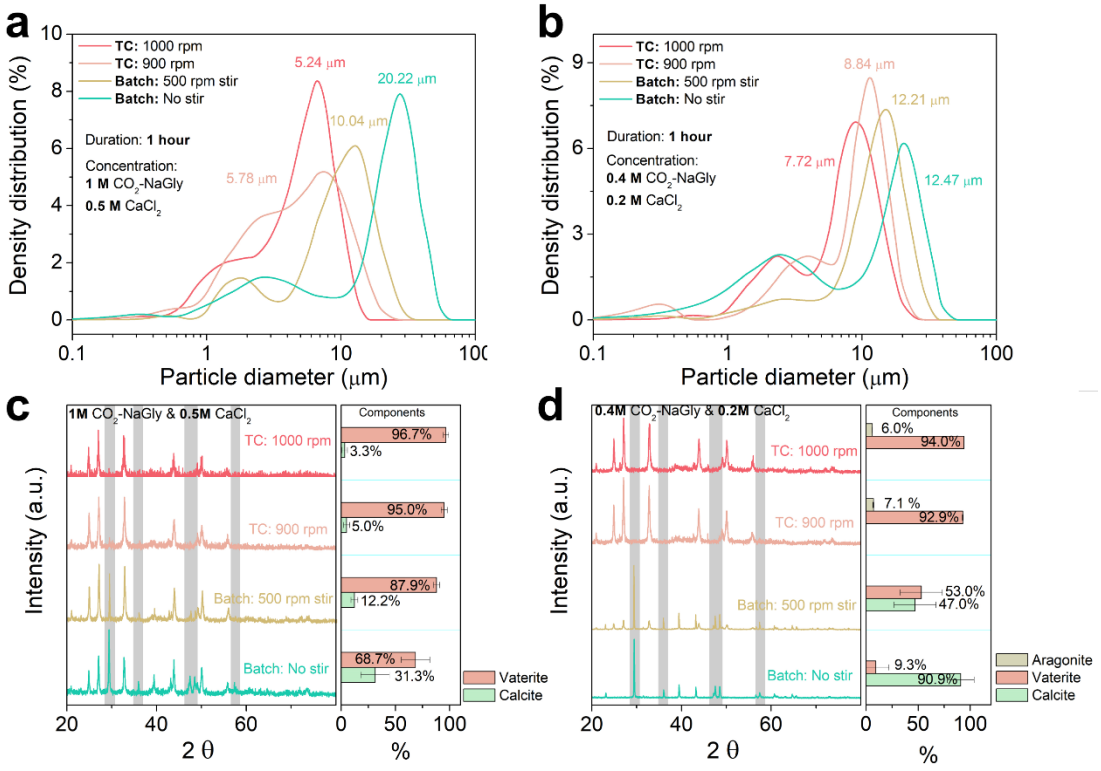

Figure 4. Particle size distribution of $CaCO_3$ produced in CT mode and batch mode at concentrations of (a) **1 M** CO_2-NaGly /**0.5 M** $CaCl_2$ (1 M/0.5 M) and (b) **0.4 M** CO_2-NaGly / **0.2 M** $CaCl_2$ (0.4 M/0.2 M). The operation duration for both modes is **1 h**. The corresponding XRD patterns at (c) high concentration (1 M/0.5 M) and (d) low concentration (0.4 M/0.2 M), respectively. (Gray shadows highlight characteristic peaks of calcite)

In general, the process of $CaCO_3$ precipitation can be divided into three main stages: (1) nucleation of amorphous calcium carbonate (ACC) in the early stage; (2) dissolution of unstable ACC and recrystallization into vaterite and calcite; (3) dissolution of the metastable vaterite and recrystallization into the most sable crystalline structure, calcite.[31, 32] It is worth noting that other metastable structures such as aragonite can form under certain conditions, including **saturation levels, temperature, pH, and reactor configurations**.[26, 33, 34]

The crystal structures of carbonate products are further investigated by X-ray diffraction (XRD). Figure 4c shows XRD patterns of products obtained under high concentrations (**1 M** CO_2-NaGly /**0.5 M** $CaCl_2$). When the reaction is conducted in batch mode, the formation of both calcite (PDF #98-000-0141) and vaterite (PDF #98-001-9636) is observed. In particular, the proportion of calcite is as high as 31.3% in batch mode with no stir (Figure 4c, right). In contrast, when the reaction is performed in the TC mode, only trace amounts of calcite can be observed (3.3 – 5.0%), and instead, more than 95% vaterite are detected at various rotational speeds. This indicates that vaterite is favorable to form in the TC mode. At lower concentrations, a similar trend from relatively more calcite to relatively more vaterite can be observed when transitioning from batch mode to TC mode (Figure 4d). In this scenario, high-purity vaterite (> 92%) is obtained when the reaction is carried out under TC mode. Both calcite and vaterite are obtained under batch mode (Figure 4d, right). These results indicates that intensive stir or Taylor vortices help the formation of micro- or nano-sized vaterite ($CaCO_3$), which is in line with existing studies.[35] In conclusion, the observed preference for vaterite production in the TC mode suggests that TC reactor helps to inhibit the further transformation of vaterite into calcite, which is the most stable crystalline form of $CaCO_3$.

3.3 Effect of Duration and Rotational Speed

It is reported that an increased rotation of the inner cylinder, or enhanced axial flow can obviously reduce the mean crystal size of the precipitate.[36, 37] As shown in Figure 5a & Figure 5b, the results are obtained from a continuous flow in TC mode with a flow rate of 3.76 mL/s, given a residence time of about 30 s. It is clear that the particle size distribution and mean size decreases as rotational speed increases. Under higher initial reactant concentrations, the mean particle size decreased from 5.14 μm to 3.05 μm with an increase in rotational speed (Figure 5a). A similar trend can be observed under lower initial reactant concentrations (Figure 5b). XRD patterns confirm that most crystals (>92%) of the products can be ascribed to vaterite (Figure S3).

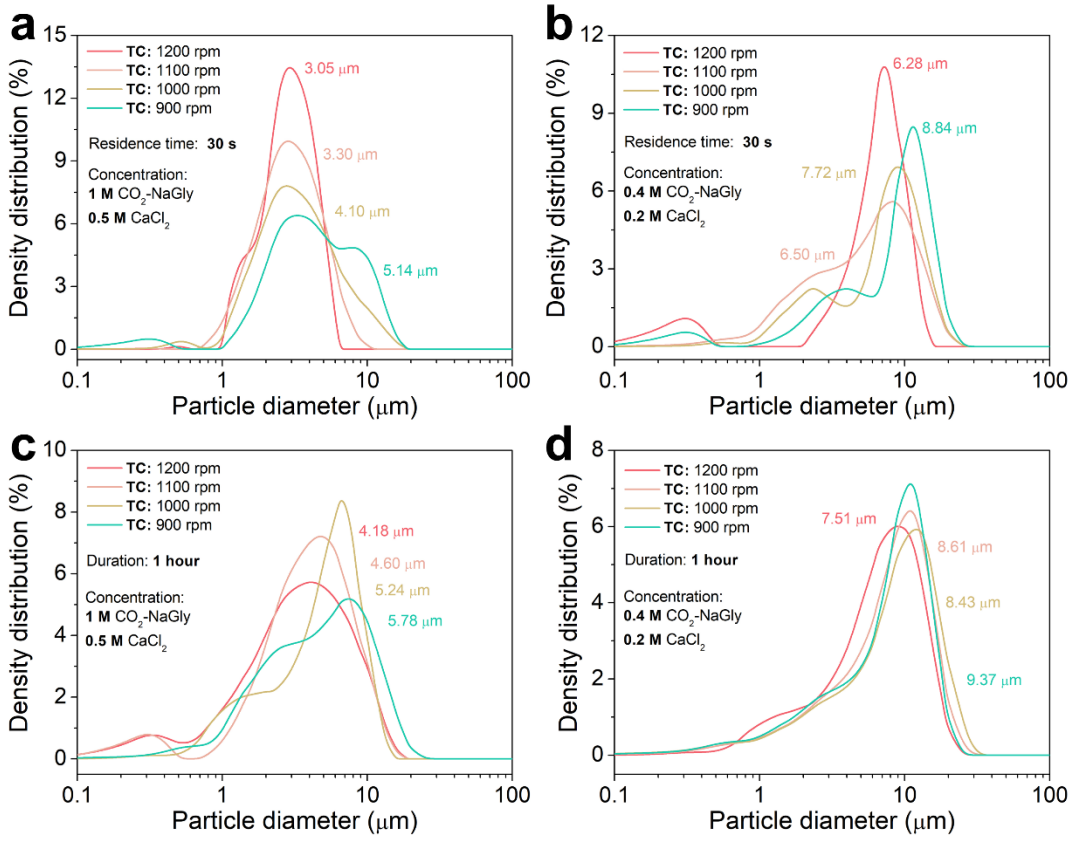

Figure 5. Particle size distribution of calcium carbonate generated in TC mode with residence time of 30 seconds for (a) **1 M** CO_2-NaGly / **0.5 M** $CaCl_2$ (1 M/0.5 M) and (b) **0.4 M** CO_2-NaGly / **0.2 M** $CaCl_2$ (0.4 M/0.2 M). Extended duration to 1 h for (c) 1 M/0.5 M and 0.4 M/0.2 M, respectively. [What do Figures (c) and (d) represent? Indicate here]

However, the peak of the particles size distributions slightly shifts towards the right, indicating larger mean sizes, when the duration extended to 1 h from 30s. The mean particle sizes increase to the range of 4.18 – 5.78 μm when subjected to the same range of rotation rates (900 – 1200 rpm) at 1 M/0.5 M concentrations (Figure 5c). Similarly, at lower concentrations, the mean particle size increases to the range of 7.51 – 9.37 μm (Figure 5d). The particle size distributions are significantly broader than those of short-time counterpart (Figure 5a & Figure 5b). All these results indicate that the effect of particle growth and agglomeration become more serious with duration of mixing at the TC mode.

Additionally, the effect of residence time in continuous TC mode is more precisely examined. It is found that residence time does not have a significant impact on particle size distribution when low rotation rates of 900 rpm (Figure S4a) and 1000 rpm (Figure S4b) are employed. However, the effect becomes more evident when high rotational speeds are applied. As shown in Figure S4, various residence times were examined, including 59, 30, 20, 15, and 12 s (corresponding to the flow rates of 1.88, 3.76, 5.64, 7.52, 9.40 mL/s for both Ca^{2+} and CO_2-NaGly solutions). When mild rotational speeds (900 & 1000 rpm) are applied, small differences in particle size distribution are observed (Figure S4a & Figure S4b). However, when a higher rotational speed (1100 & 1200 rpm) is applied, longer residence times typically result in significantly smaller particle sizes (Figure S4c & Figure S4d). For example, under the rotational speed of 1200 rpm, a residence time of 59 s yields a mean particle size as small as 4.24 μm. This size is approximately 40% smaller than the mean particle size obtained with a residence time of 12 s (5.95 μm). It is important to note that all measured particle sizes tend to decrease with increasing rotational speed.

3.4 Analysis of Morphology of the Particles

The morphology of the produced carbonates in both the TC mode and batch mode is further investigated by scanning electron microscope (SEM). In the case of high concentrations (**1 M** CO_2-NaGly / **0.5 M** $CaCl_2$), a sphere-like morphology that can be attributed to vaterite particles are observed with the TC mode.[22] This confirms the initial XRD results which indicated that the majority of the crystalline structures can be attributed to vaterite, accounting for over 95% of the total crystalline content, while a small portion corresponds to calcite, comprising less than 5% (Figure S3). As shown in Figure 6a, a spherical particle with a rough surface was observed with the TC mode at a rotation rate of 900 rpm. As the rotational speed increases, the surface of formed particles becomes noticeably rougher (Figure b-d). The fine grains that make up the particles become smaller. Generally, higher shear stress results in less aggregation, narrower floc size distribution and higher fractal dimension.[14] In batch mode, however, irregular structures are co-produced alongside sphere-like vaterite. Although, the sphere-like particles were dominant in products when a stirring rate of 500 rpm is applied. As shown in Figure 6e, most sphere-like particles (vaterite) exhibit sizes

exceeding 6 μm, whereas a small portion of irregular structures (Figure 6f), which may constitute calcite and aragonite, intermingled with vaterite. Note that the produced sphere-like vaterite exhibits a smooth surface, lacking apparent fine grains. This morphology looks very different from those observed with the TC mode. Moreover, larger particles and more irregular structures are observed when no stirring is provided. Figure 6g displays a typical sphere-like particle with smoother and sheen surface. Meanwhile, the particles with rough surfaces (Figure 6h), distinct from the smooth counterparts, can be observed. This morphology is characteristic of calcite, which aligns with the XRD results (Figure 4c). In conclusion, we hypothesize that the inhomogeneous hydrodynamics with the batch mode leads to different localized shear rates, causing more serious aggregation. The intrinsic variations result in different steps of breakage and regrowth on the aggregate size and morphology.[38] In contrast to the inhomogeneity observed in the batch mode, the TC mode can offer better shear stresses leading to better control of particle properties.[39]

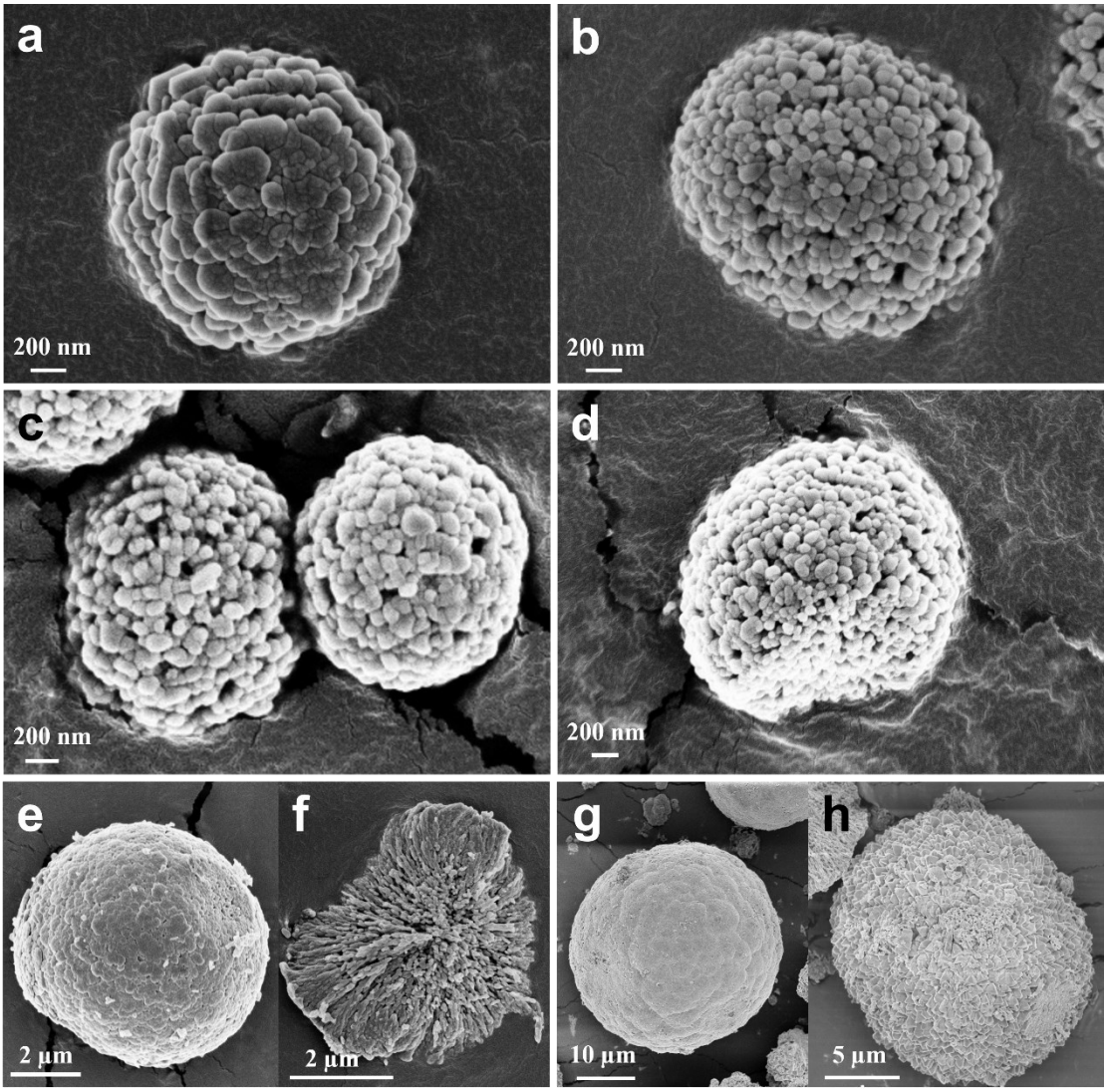

Figure 6. Morphological features of $CaCO_3$ particles using SEM images obtained in TC mode with residence time of 30 seconds under various rotation rates: (a) 900 rpm, (b) 1000 rpm, (c) 1100 rpm, (d) 1200 rpm; and in batch mode with (e, f) 500 rpm stir and (g, h) no stirring. Experiments are conducted using **1 M** CO_2 loaded Na-glycinate and **0.5 M** $CaCl_2$ solution.

Furthermore, particle sizes were measured based on zoom-out SEM images which contains over 50 measurable particles. As shown in Figure S5, global images and corresponding histograms of particle size indicate that higher rotational speed in the TC mode tends to generate smaller particles with rougher surfaces. Figure S5a, which is the zoom-out image of Figure 6a, shows quite a few recognizable spherical particles. These particles exhibit a size range from 0.63 µm to 2.75 µm, as depicted in Figure S5b.

At a rotational speed of 1200 rpm, in contrast, the smallest mean size of 1.4 μm, compared to sizes of 1.70 μm, 1.47 μm, and 1.43 μm at 900 rpm, 1000 rpm, and 1100 rpm, respectively, is noted (Figure S5c-h). Note that with the increasing rotational speed, the sphere-like vaterite products tend to be smaller in size. Therefore, it can be concluded that TC mode can generate sphere-like vaterite particles with more uniform particle sizes.

This clear trend in the particle size distribution is consistent with the previous PSA results measured by laser. But there seems to be a notable disparity between the particle sizes observed in SEM images and the results obtained from the particle size analyzer (PSA) in Figure 5a. This shift towards relatively larger particle sizes observed in PSA may be attributed to agglomeration, as evidenced by the observation of agglomerated particles in SEM images. This phenomenon of particles clumping together leads to influence the observation of larger particle sizes (PSA) compared to the individual particle sizes measured by SEM (which has been discussed in Figure 3). Besides, employing distinct normalization techniques, namely volume-weighted and number-weighted, yields varying distribution patterns.

In the case of low initial concentrations (**0.4 M** CO_2-Na-gGly / **0.2 M** $CaCl_2$), sphere-like particles can also be observed, however, these conditions exhibit larger particle size and variance. Figure S6 illustrates the formation of similar sphere-like particles, characterized by smoother surfaces (compared with the particles obtained from high-concentration conditions). In contrast to high concentrations, significantly larger particle sizes are observed. Specifically, the mean particle sizes across all rotation rates studied ranged from 4.16 to 5.16 μm, which is at least 2.5 times larger than those observed in high concentrations. In addition, a noticeable variance in particle size can be observed (Figure S6c, Figure S6f, Figure S6i). This indicates that relatively less uniform particle sizes are generated at low concentrations, despite the formation of similar sphere-like products. Moreover, the irregular morphology of calcite products appears to be dominant with batch mode (Figure S7). Although sphere-like particles are still observed when stirring is applied, there is a significant presence of larger irregular particles (Figure S7a). These irregular calcite particles, some reaching sizes as large as 27 μm in size (highlighted in a yellow circle), are frequently observed alongside the sphere-like particles (Figure S7b & Figure S7c). Also, it appears that most of the sphere-like vaterite particles exhibit a higher degree of defects with low reactant

concentration compared to those observed in high concentrations. When no stirring was provided, nearly all particles are composed of calcite, which possess the roughest surfaces among all the cases (Figure S7d). More typical features associated with calcite can be observed in the zoomed-in SEM image (Figure S7e).

Elongated calcite crystals can be observed with an extended operation time (1 h) in the TC mode. As shown in Figure S8, prismatic crystals are formed at various rotational speeds, which are not seen during the short residence time (30 s, Figure 6). This is in agreement with the XRD results (Figure 4d). Besides, the zoomed-in images prove the formation of defective vaterite particles and some noticeably small grains. It can be ascribed to the persistent influence of the Taylor vortices, which somewhat hinder the growth and agglomeration of nuclei. In addition, prismatic calcite crystals are more likely to form at longer reactor residence time.

3.5 Effect of Alkaline Industrial Leachates

Alkaline industrial leachates can be utilized as Ca- or Mg-bearing sources for carbonate production via CO_2 mineralization.[2, 22] In this study, two different leachates, *USFe* leachate (a slag from the iron industry) and waste *Concrete* leachate (construction waste), are employed as Ca sources for $CaCO_3$ precipitation. Unlike pure Ca^{2+} sources, alkaline industrial leachates contain foreign ions, which can influence the process of precipitation. The presence of foreign ions is likely to generate interaction within the $CaCO_3$ cluster, leading to a reduced nucleation rate. Moreover, foreign ions can also interact with the surface of precipitated carbonate particles, thus probably blocking some crystal-growing planes. Not surprisingly, the kinetics and crystal formation mechanism could be influenced, leading to products with distinct characteristics.[40]

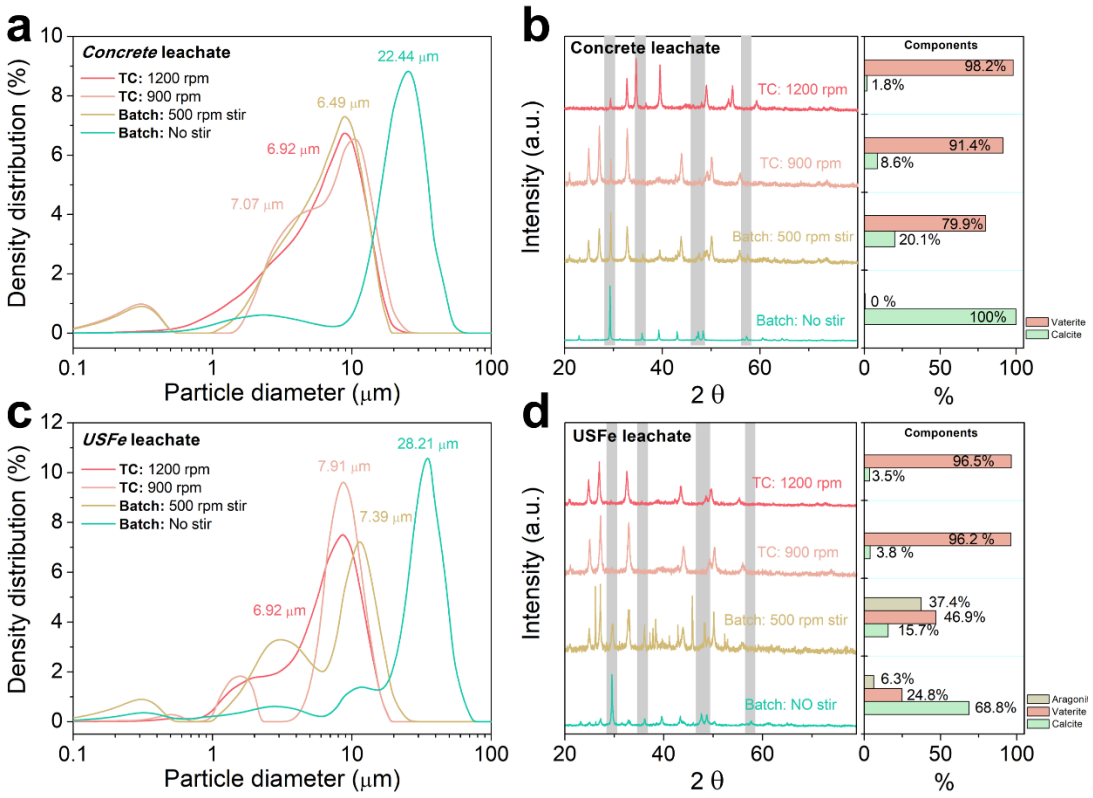

Figure 8. Particle size distribution patterns of calcium carbonate produced from (a) *Concrete* leachate and (b) corresponding XRD patterns. Particle size distribution patterns of carbonates produced from (c) *USFe* leachate and (d) corresponding XRD patterns. [Indicate experimental conditions here]

In this study, *Concrete leachate* and *USFe leachate* are used to elucidate the effect of impurities on the morphology and chemical structure of $CaCO_3$ products. The preparation methods of these two leachates are discussed in the Materials and Methods section (Section 2). Based on the results from ICP, the leachate sample contains mostly Ca ions, as well as small portions of Mg, Fe, and so on. In the both cases, **1 M** CO_2-loaded NaGly is utilized. PSA is first carried out to study particle size distribution in both TC and batch modes. When *Concrete leachate* serves as Ca^{2+} source, the produced particles in TC mode exhibit smaller particle mean size and narrower size distribution, especially compared to the batch mode with no stir (Figure 8a). Note that when stirring is supplied in batch mode, the particle distribution appears to be similar to those observed in the TC mode. However, the differences lie in crystalline structure and morphology. As shown in Figure 8b, a considerable amount of calcite (>20%) is

observed alongside the vaterite. In terms of morphology, most of the observed carbonate particles produced in TC mode has sphere-like shape, while prismatic crystals along with small irregular particles can be observed in the batch mode (Figure S9). Moreover, the carbonate particles generated in TC-mode display greater smoothness, with no apparent presence of fine grains on the surface. It is worth noting that the uniformity of particles obtained by *Concrete leachate* is significantly less than those obtained by pure Ca^{2+} sources. These results may probably be caused by the presence of foreign ions in the leachate, including significant abundance of Mg. The kinetics of nucleation, growth, and agglomeration for the precipitation of $CaCO_3$ can be influenced by the existing ions, leading to changes in nucleation, growth and agglomeration constants.[3, 40] Similar results are observed by utilizing *USFe leachate* (Figure 8c). However, while most vaterite is formed in the TC mode, the formation of aragonite alongside calcite and vaterite are observed for the *USFe* carbonates in the batch mode (Figure 8d). SEM images show that most observed carbonate particles produce in the TC mode are in sphere-like shape with greater smoothness compared to those produced by using pure Ca^{2+} sources (Figure S10). However, prismatic crystals along with small irregular particles can be observed in the batch mode. Note that even though similar particles size distributions are observed for TC mode and batch with stirring, their morphology and crystalline structures are totally different. In summary, leachates derived from alkaline industrial waste, despite containing various foreign ions, can serve as Ca sources for the production of sphere-like vaterite using a TC reactor.

Conclusion

In this study, a Taylor-Couette Carbonate Conversion reactor (TC^3) is elaborately adapted to produce precipitated calcium carbonate (PCC). Taylor-Couette vortices was found to play a significant role in the formation of carbonate particles with ultrafine size and fine-tuned morphology. In detail, narrower particle size distribution in a range of 0.2 – 10 μm can be obtained with TC^3, compared to 0.1 – 64 μm obtained with a batch reactor. Moreover, sphere-like vaterite particles with more uniform particle size and high crystalline purity are produced via TC^3. An evolution of crystal structure from calcite to vaterite occurs along with the change of the flow pattern from conventional stirring to Taylor vortices. Meanwhile, the corresponding changes of particle size and morphology indicate the feasibility of producing desired particle properties by the modulation of the reaction conditions. In the condition of Taylor-Couette flow, the obtained carbonate products tend to be more uniformly sized and possess higher purity with increasing rotational strength and reasonable residence time. It is worth noting that similar trends can also be observed when using alkaline industrial leachates as a Ca bearing source. However, the presence of foreign ions can significantly influence the characteristics of PCC, involving particle size, roughness, shape and so on. In summary, all results indicate that the vortex-CO_2 technology has a great potential to address the societal need of utilizing multiple waste streams such as alkaline industrial residues and anthropogenic CO_2 to produce value-added products. It sheds light on an efficient and commercially realizable process for producing value-added inorganic carbonates from captured CO_2.

Conflicts of Interest

There is no confit of interest to declare.

Acknowledgement

The authors acknowledge the use of the shared facilities at the Cornell Center for Materials Research (CCMR), which are supported through the NSF MRSEC program (DMR-1719875). We would like to thank Nadine Piatak, a research geologist with USGS Geology, Energy & Minerals (GEM) Science Center in Reston, Virginia for providing us with industrial residues used for this study.

References

1. Gadikota, G., Carbon mineralization pathways for carbon capture, storage and utilization. *Communications Chemistry* **2021,** *4* (1), 23.
2. Gadikota, G., Multiphase carbon mineralization for the reactive separation of CO_2 and directed synthesis of H2. *Nature Reviews Chemistry* **2020,** *4* (2), 78-89.
3. Liendo, F.; Arduino, M.; Deorsola, F. A.; Bensaid, S., Factors controlling and influencing polymorphism, morphology and size of calcium carbonate synthesized through the carbonation route: A review. *Powder Technology* **2022,** *398*, 117050.
4. Simkiss, K., Variations in the Crystalline Form of Calcium Carbonate precipitated from Artificial Sea Water. *Nature* **1964,** *201* (4918), 492-493.
5. Svenskaya, Y. I.; Fattah, H.; Inozemtseva, O. A.; Ivanova, A. G.; Shtykov, S. N.; Gorin, D. A.; Parakhonskiy, B. V., Key Parameters for Size- and Shape-Controlled Synthesis of Vaterite Particles. *Crystal Growth & Design* **2018,** *18* (1), 331-337.
6. Trushina, D. B.; Bukreeva, T. V.; Kovalchuk, M. V.; Antipina, M. N., $CaCO_3$ vaterite microparticles for biomedical and personal care applications. *Materials Science and Engineering: C* **2014,** *45*, 644-658.
7. Ming-Guo, M.; Run-Cang, S., Biomineralization and Biomimetic Synthesis of Biomineral and Nanomaterials. In *Advances in Biomimetics*, Anne, G., Ed. IntechOpen: Rijeka, 2011; p Ch. 2.
8. Ohgushi, H.; Okumura, M.; Yoshikawa, T.; Inboue, K.; Senpuku, N.; Tamai, S.; Shors, E. C., Bone formation processin porous calcium carbonate and hydroxyapatite. *Journal of Biomedical Materials Research* **1992,** *26* (7), 885-895.
9. Hargis, C. W.; Telesca, A.; Monteiro, P. J. M., Calcium sulfoaluminate (Ye'elimite) hydration in the presence of gypsum, calcite, and vaterite. *Cement and Concrete Research* **2014,** *65*, 15-20.
10. Wang, L. K.; Vaccari, D. A.; Li, Y.; Shammas, N. K., Chemical Precipitation. In *Physicochemical Treatment Processes*, Wang, L. K.; Hung, Y.-T.; Shammas, N. K., Eds. Humana Press: Totowa, NJ, 2005; pp 141-197.
11. Bałdyga, J.; Podgórska, W.; Pohorecki, R., Mixing-precipitation model with application to double feed semibatch precipitation. *Chemical Engineering Science* **1995,** *50* (8), 1281-1300.
12. Kang, S. H.; Lee, S. G.; Jung, W. M.; Kim, M. C.; Kim, W.-S.; Choi, C. K.; Feigelson, R. S., Effect of Taylor vortices on calcium carbonate crystallization by gas–liquid reaction. *Journal of Crystal Growth* **2003,** *254* (1), 196-205.
13. Aljishi, M. F.; Ruo, A.-C.; Park, J. H.; Nasser, B.; Kim, W.-S.; Joo, Y. L., Effect of flow structure at the onset of instability on barium sulfate precipitation in Taylor–Couette crystallizers. *Journal of Crystal Growth* **2013,** *373*, 20-31.
14. Schrimpf, M.; Esteban, J.; Warmeling, H.; Färber, T.; Behr, A.; Vorholt, A. J., Taylor-Couette reactor: Principles, design, and applications. *AIChE Journal* **2021,** *67* (5), e17228.
15. Calcium Carbonate Market Size, Share & Trends Analysis Report By Type (GCC, PCC), By Application (Automotive, Building & Construction, Pharmaceutical, Agriculture, Pulp & Paper), By Region, And Segment Forecasts, 2023 - 2030. https://www.grandviewresearch.com/industry-analysis/calcium-carbonate-market (accessed June 6, 2023).
16. Global Magnesium Carbonate Market Research Report 2020. https://www.marketreportsworld.com/global-magnesium-carbonate-market-14316818 (accessed June 29, 2023).
17. Liu, M.; Hohenshil, A.; Gadikota, G., Integrated CO2 Capture and Removal via Carbon Mineralization with Inherent Regeneration of Aqueous Solvents. *Energy & Fuels* **2021,** *35* (9), 8051-8068.

18. Guo, D.; Thee, H.; Tan, C. Y.; Chen, J.; Fei, W.; Kentish, S.; Stevens, G. W.; da Silva, G., Amino Acids as Carbon Capture Solvents: Chemical Kinetics and Mechanism of the Glycine + CO2 Reaction. *Energy & Fuels* **2013,** *27* (7), 3898-3904.
19. Vaidya, P. D.; Konduru, P.; Vaidyanathan, M.; Kenig, E. Y., Kinetics of Carbon Dioxide Removal by Aqueous Alkaline Amino Acid Salts. *Industrial & Engineering Chemistry Research* **2010,** *49* (21), 11067-11072.
20. Brethomé, F. M.; Williams, N. J.; Seipp, C. A.; Kidder, M. K.; Custelcean, R., Direct air capture of CO2 via aqueous-phase absorption and crystalline-phase release using concentrated solar power. *Nature Energy* **2018,** *3* (7), 553-559.
21. Custelcean, R.; Williams, N. J.; Garrabrant, K. A.; Agullo, P.; Brethomé, F. M.; Martin, H. J.; Kidder, M. K., Direct Air Capture of CO2 with Aqueous Amino Acids and Solid Bis-iminoguanidines (BIGs). *Industrial & Engineering Chemistry Research* **2019,** *58* (51), 23338-23346.
22. Yin, T.; Yin, S.; Srivastava, A.; Gadikota, G., Regenerable solvents mediate accelerated low temperature CO2 capture and carbon mineralization of ash and nano-scale calcium carbonate formation. *Resources, Conservation and Recycling* **2022,** *180*, 106209.
23. Ochonma, P.; Noe, C.; Mohammed, S.; Mamidala, A.; Gadikota, G., Integrated low carbon H2 conversion with in situ carbon mineralization from aqueous biomass oxygenate precursors by tuning reactive multiphase chemical interactions. *Reaction Chemistry & Engineering* **2023**.
24. Taylor, G. I., Stability of a Viscous Liquid Contained between Two Rotating Cylinders. *Philosophical Transactions of the Royal Society of London. Series A, Containing Papers of a Mathematical or Physical Character* **1923,** *223*, 289-343.
25. Taylor, G. I., Fluid friction between rotating cylinders I—Torque measurements. *Proceedings of the Royal Society of London. Series A - Mathematical and Physical Sciences* **1936,** *157* (892), 546-564.
26. Chang, R.; Choi, D.; Kim, M. H.; Park, Y., Tuning Crystal Polymorphisms and Structural Investigation of Precipitated Calcium Carbonates for CO2 Mineralization. *ACS Sustainable Chemistry & Engineering* **2017,** *5* (2), 1659-1667.
27. Jung, W.-M.; Hoon Kang, S.; Kim, K.-S.; Kim, W.-S.; Kyun Choi, C., Precipitation of calcium carbonate particles by gas–liquid reaction: Morphology and size distribution of particles in Couette-Taylor and stirred tank reactors. *Journal of Crystal Growth* **2010,** *312* (22), 3331-3339.
28. Jung, W. M.; Kang, S. H.; Kim, W.-S.; Choi, C. K., Particle morphology of calcium carbonate precipitated by gas–liquid reaction in a Couette–Taylor reactor. *Chemical Engineering Science* **2000,** *55* (4), 733-747.
29. Schwarzer, H.-C.; Peukert, W., Combined experimental/numerical study on the precipitation of nanoparticles. *AIChE Journal* **2004,** *50* (12), 3234-3247.
30. Wójcik, J. A.; Jones, A. G., Experimental Investigation into Dynamics and Stability of Continuous MSMPR Agglomerative Precipitation of CaCO3 Crystals. *Chemical Engineering Research and Design* **1997,** *75* (2), 113-118.
31. Bots, P.; Benning, L. G.; Rodriguez-Blanco, J.-D.; Roncal-Herrero, T.; Shaw, S., Mechanistic Insights into the Crystallization of Amorphous Calcium Carbonate (ACC). *Crystal Growth & Design* **2012,** *12* (7), 3806-3814.
32. Rodriguez-Blanco, J. D.; Shaw, S.; Benning, L. G., The kinetics and mechanisms of amorphous calcium carbonate (ACC) crystallization to calcite, viavaterite. *Nanoscale* **2011,** *3* (1), 265-271.
33. Wang, B.; Pan, Z.; Cheng, H.; Chen, Z.; Cheng, F., High-yield synthesis of vaterite microparticles in gypsum suspension system via ultrasonic probe vibration/magnetic stirring. *Journal of Crystal Growth* **2018,** *492*, 122-131.
34. Udrea, I.; Capat, C.; Olaru, E. A.; Isopescu, R.; Mihai, M.; Mateescu, C. D.; Bradu, C., Vaterite Synthesis via Gas–Liquid Route under Controlled pH Conditions. *Industrial & Engineering Chemistry Research* **2012,** *51* (24), 8185-8193.

35. Luo, X.; Song, X.; Cao, Y.; Song, L.; Bu, X., Investigation of calcium carbonate synthesized by steamed ammonia liquid waste without use of additives. *RSC Advances* **2020,** *10* (13), 7976-7986.
36. Judat, B.; Racina, A.; Kind, M., Macro- and Micromixing in a Taylor-Couette Reactor with Axial Flow and their Influence on the Precipitation of Barium Sulfate. *Chemical Engineering & Technology* **2004,** *27* (3), 287-292.
37. Nguyen, A.-T.; Joo, Y. L.; Kim, W.-S., Multiple Feeding Strategy for Phase Transformation of GMP in Continuous Couette–Taylor Crystallizer. *Crystal Growth & Design* **2012,** *12* (6), 2780-2788.
38. Guérin, L.; Coufort-Saudejaud, C.; Liné, A.; Frances, C., Dynamics of aggregate size and shape properties under sequenced flocculation in a turbulent Taylor-Couette reactor. *Journal of Colloid and Interface Science* **2017,** *491*, 167-178.
39. Vlieghe, M.; Coufort-Saudejaud, C.; Frances, C.; Liné, A., In situ characterization of floc morphology by image analysis in a turbulent Taylor–Couette reactor. *AIChE Journal* **2014,** *60* (7), 2389-2403.
40. Alamdari, A.; Alamdari, A.; Mowla, D., Kinetics of calcium carbonate precipitation through CO2 absorption from flue gas into distiller waste of soda ash plant. *Journal of Industrial and Engineering Chemistry* **2014,** *20* (5), 3480-3486.